Acta Pharmaceutica Sinica B 2021;11(2):534–543

Chinese Pharmaceutical Association
Institute of Materia Medica, Chinese Academy of Medical Sciences

Acta Pharmaceutica Sinica B

www.elsevier.com/locate/apsb
www.sciencedirect.com

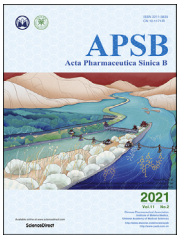

ORIGINAL ARTICLE

Cryptobiosis-inspired assembly of "AND" logic gate platform for potential tumor-specific drug delivery

Hu Zhou[a,†], Gang He[b,†], Yanbin Sun[b], Jingguo Wang[b], Haitao Wu[b], Ping Jin[a,*], Zhengbao Zha[b,*]

[a]*Shenzhen Maternity and Child Healthcare Hospital, Shandong University, Shenzhen 518028, China*
[b]*School of Food and Biological Engineering, School of Instrument Science and Opto-Electronics Engineering, Hefei University of Technology, Hefei 230009, China*

Received 27 April 2020; received in revised form 2 July 2020; accepted 18 July 2020

KEY WORDS

Cryptobiosis;
"AND" logic gate;
Polyphenol–metal chemistry;
Drug delivery;
Tumor microenvironment

Abstract Developing tumor-specific drug delivery systems with minimized off-target cargo leakage remains an enduring challenge. In this study, inspired from the natural cryptobiosis explored by certain organisms and stimuli-responsive polyphenol–metal coordination chemistry, doxorubicin (DOX)-conjugated gelatin nanoparticles with protective shells formed by complex of tannic acid and Fe^{III} (DG@TA-Fe^{III} NPs) were successfully developed as an "AND" logic gate platform for tumor-targeted DOX delivery. Moreover, benefiting from the well-reported photothermal conversion ability of TA-Fe^{III} complex, a synergistic tumor inhibition effect was confirmed by treating 4T1 tumor-bearing mice with DG@TA-Fe^{III} NPs and localized near-infrared (NIR) laser irradiation. As a proof of concept study, this work present a simple strategy for developing "AND" logic gate platforms by coating enzyme-degradable drug conjugates with detachable polyphenol–metal shells.

*Corresponding authors.
E-mail addresses: pingjin68@smu.edu.cn (Ping Jin), zbzha@hfut.edu.cn (Zhengbao Zha).
[†]These authors make equal contributions to this work.

Peer review under responsibility of Chinese Pharmaceutical Association and Institute of Materia Medica, Chinese Academy of Medical Sciences.

https://doi.org/10.1016/j.apsb.2020.08.007

1. Introduction

In the past decades, innovations in the development of targeted and controlled drug delivery vehicles could always exhilarate scientists for overcoming the lack of specificity of conventional chemotherapeutic agents and combating life-threatening diseases[1]. Although promising in preclinical animal models, the stochastic nature of ligand−receptor interactions *in vivo* and non-specific Fickian diffusion-governed drug leakage before arriving at pathological regions still remain the main barriers for clinical translation of these reported drug carriers[2−5]. Recently, due to the altered metabolic pathways and/or pathological microenvironment, exploiting drug vehicles that are sensitive to disease-associated biochemical markers (such as dysregulated pH, enzymes and redox balance) has been preferred for liberating cargos in a particular area with efficient spatial, temporal and dosage control[6−8]. Frustratingly, it is still a tremendous challenge to realize accurate drug delivery triggered by a single biomarker which is rarely unique in the diseased area[9]. Despite dual/multi-stimuli responsive systems have been further designed for accelerating the offloading of therapeutic drugs, the commonly utilized "OR" logic gates always lead to adverse off-target drug leakage on the way activated by each stimulus in complex biological milieu[10−15]. For instance, Amir et al.[16] reported the application of the logic gate concept to engineer a two enzymatic reaction-triggered drug release system. Although the presence of either of the enzymes would be sufficient to open the switch of the "drug releasing gate", but the "OR" logic would also increase the risk of premature drug release before arriving at disease regions. Inspired by the Boolean logic idea, "AND" logic gate-based systems are favored for sequence-activated drug release in pathological sites with desired specificity[17−20]. Wei et al.[21] developed an "AND" logic gate drug delivery system with two orthogonal molecular triggers (acidic pH and reduction) based on dithiodiethanoic acid crosslinked PEO-*b*-P(MAA-*g*-Hyd) block copolymer micelles conjugated with adriamycin drug through the hydrazone bonds. Despite promising and effective, subjected to the inherent constraints on material composition and vehicle geometry, the uniqueness of each previously reported "AND" logic gate-based platform invariably necessitates a brand new material design that is generally not synthetically tractable[22]. Therefore, a versatile strategy for the construction of "AND" logic gate-based platform was highly pursued for programmed disease-specific drug delivery with minimized off-target effect.

Cryptobiosis, also known as "secret life", has been developed in nature by certain bacteria, ciliates and even higher organisms (*e.g.*, tardigrades) as well as seeds of some plants to withstand stressful and often lethal environmental conditions[23−25]. This cytoprotective strategy commonly involves the formation of tough biomolecular sheaths on cellular structures to enter a dormant state for survival from outside threats and subsequent revival to proliferate by breaking the protective shells apart when the environment becomes favorable[26,27]. Inspired from this fascinating cryptobiotic mechanism, chemically forming a thin (<100 nm) but durable shell on living cells (cell-in-shell structures) have been demonstrated to be effective for enhancing tolerance against harmful threats as well as controlled cellular metabolism which are anticipated to find various applications in biomedical areas including biocatalysis, cytotherapeutics and single-cell biology[28−30]. For instance, individual labile mammalian/microbial yeast cell has been evolved into a micrometer-sized "Iron Man" by coating with polyphenol–metal complexes comprised of natural polyphenol tannic acid (TA) and Fe^{III} for customizable cellular adherence and proliferation as a consequence of programmed shell formation and degradation[31,32]. Yet, in contrast to the flourishing research situation for cell-in-shell structures, developing cryptobiotic systems with "AND" logic gate behaviors for sequence-activated drug delivery have been rarely reported.

As a proof-of-concept study, a cryptobiosis inspired assembly of pH/ATP "AND" enzyme logic gate platform was successfully developed here to realize tumor-specific drug delivery. As shown in Scheme 1A, after conjugating chemotherapeutic doxorubicin hydrochloride (DOX·HCl) molecules on the surface of gelatin nanoparticles (DG NPs) through typical aldimine condensation, conformal TA-Fe^{III} shell was subsequently deposited on the surface of DG NPs (DG@TA-Fe^{III} NPs) for realizing "AND" logic gate-controlled drug delivery in tumor regions. By preventing the contact between DG NPs and enzyme with durable TA-Fe^{III} shells in healthy tissues, the obtained DG@TA-Fe^{III} NPs were expected to exhibit a cryptobiotic behavior with negligible premature drug leakage. Once arrived at tumor regions, the mild acidic pH and/or upregulated adenosine triphosphate (ATP) in the tumor microenvironment would firstly unlock the TA-Fe^{III} shells and then the subsequently exposed inner DG cores could be hydrolysed by overexpressed matrix metalloproteinase 2/9 (MMP 2/9, also known as gelatinase) in solid tumor regions to release cytotoxic DOX (Scheme 1B). In addition to this "AND" logic gate-controlled DOX delivery in tumor, the good photothermal conversion activity of TA-Fe^{III} complex would endow DG@TA-Fe^{III} NPs with synergistic photothermal–chemo cell-killing ability under near-infrared (NIR) light irradiation. Benefiting from the dynamic nature of polyphenolic-metal coordinative complex, our study was anticipated to present a versatile strategy for developing "AND" logic gate-based systems for disease-specific drug delivery.

2. Materials and methods

2.1. Reagents and chemicals

Gelatin type A (from porcine skin, powder, ~300 bloom) were purchased from Sigma−Aldrich (9000-70-8, St. Louis, MO, USA). Tannin acid (TA, >99%, 1401-55-4) and iron chloride hexahydrate ($FeCl_3 \cdot 6H_2O$, >99%, 10025-77-1) were obtained from Aladdin Industrial Corporation (Shanghai, China). Acetone (67-64-1), absolute ethanol (64-17-5) and glutaraldehyde solution (GTA, 25%, 111-30-8) were received from Sinopharm Chemical Reagent Co., Ltd. (Shanghai, China). Doxorubicin hydrochloride (DOX·HCl, 480453-73-4) was bought from Beijing Huafeng United Technology Co., Ltd. (Beijing, China). All chemicals were used as received without additional purification.

2.2. Synthesis of DG NPs

Monodispersed gelatin NPs were firstly developed from a well-reported two-step desolvation process and subsequently cross-linked by GTA molecules. After mixing the DOX·HCl aqueous solution (1 mg/mL, 10 mL) with GTA solution of various feeding mass ratios (1:1, 1:5, 1:10, 1:50, and 1:100) for 2 h at room temperature, the gelatin NPs (10 mg/mL, 10 mL) were then quickly added into the aldehydated DOX suspension and stirred vigorously for further 2 h. The DG NPs could be successfully collected through typical centrifugation/washing cycles.

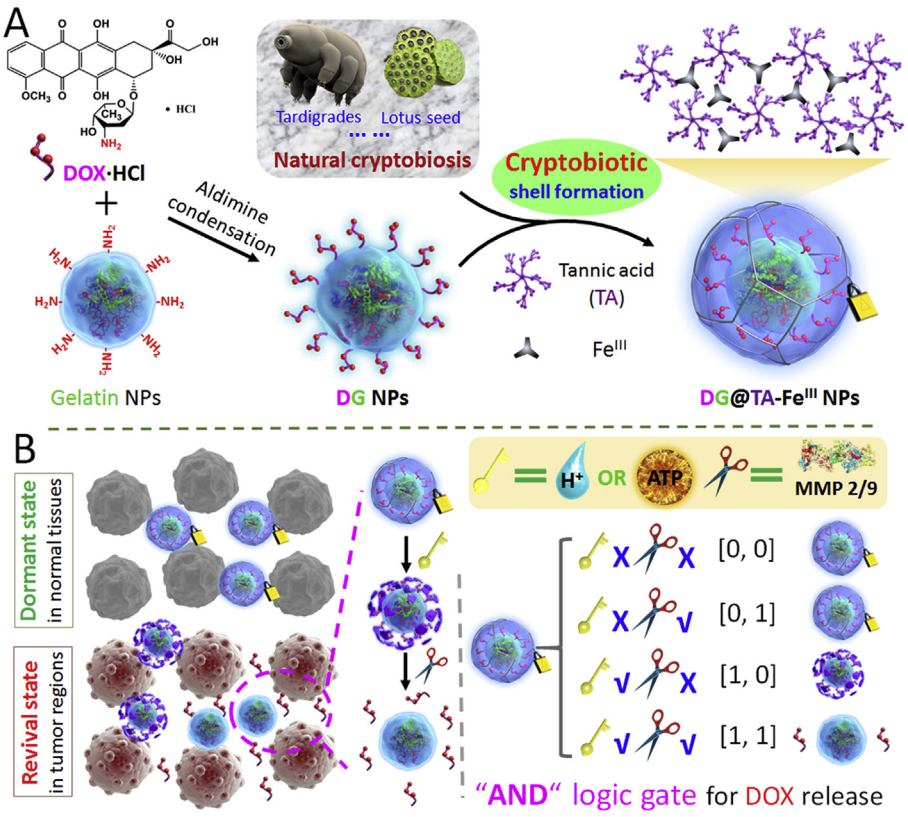

Scheme 1 Schematic illustration for (A) the preparation of cryptobiotic DG@TA-Fe^{III} NPs and (B) the underlying mechanism for "AND" logic gate controlled DOX release performance in tumor region.

2.3. *Fabrication of cryptobiotic DG@TA-Fe^{III} NPs*

The cryptobiotic DG@TA-Fe^{III} NPs were developed by subsequently depositing TA and Fe^{III} molecules on the surface of DG NPs to form conformal TA-Fe^{III} shell *via* polyphenol–metal coordination chemistry. Typically, 1 mL of TA aqueous solution (10 mg/mL) was quickly added into DG NPs suspension (100 mg, 99 mL) under vigorous stirring for 30 min. After several centrifugation/washing cycles, the collected DG@TA NPs was then resuspended in DI water (99 mL) and followed addition of $FeCl_3 \cdot 6H_2O$ solution (1 mL, 10 mg/mL). With magnetic stirring for 30 min at room temperature, the cryptobiotic DG@TA-Fe^{III} NPs could be obtained by standard purification process.

2.4. *Characterization of DG@TA-Fe^{III} NPs*

Hydrodynamic diameters and zeta potential of as-prepared NPs were measured at 25 °C by using a Zetasizer® Nano-Series instrument (Nano ZS90, Malvern Instruments Ltd., Worcestershire, UK). The ultraviolet−visible−near-infrared light (UV−Vis−NIR) absorption spectra of NPs were measured by a U-5100 UV spectrophotometer (Hitachi, Tokyo, Japan) at room temperature. The morphologies of NPs were observed by scanning electron microscope (SEM, Hitachi SU8020, Tokyo, Japan) and transmission electron microscope (TEM, JEM-2100F, JEOL, Tokyo, Japan).

2.5. *In vitro iron ion and DOX release performance*

A typical 1,10-phenanthroline chromogenic method was utilized to test the ATP/pH sensitive disassembly of TA-Fe^{III} shell. In brief, 3 mL of DG@TA-Fe^{III} NPs (1 mg/mL) was packaged in a dialysis bag with a molecular weight cut-off of 14 kDa. After immersed in 27 mL PBS with various concentrations of ATP and pH values, 3 mL of the releasing buffer was taken out and supplemented with the same volume of fresh PBS at predetermined time intervals. After adding hydroxylamine hydrochloride to the taken solution and reacting with 1,10-phenanthroline (1 mg/mL) for 15 min, the released iron ion could be calculated by measuring the absorbance at 510 nm. The released amount of DOX was also determined by incubating the sealed DG@TA-Fe^{III} NPs (1 mg/mL, 3 mL) with different stimuli (ATP, acidic pH, gelatinase).

2.6. *Photothermal conversion effect of DG@TA-Fe^{III} NPs*

Gradient concentrations of DG@TA-Fe^{III} NPs (200 μL) were irradiated for 3 min by a continuous NIR laser (MDL−III−808-2, Changchun New Industries Optoelectronics Technology Co., Ltd., Changchun, China). The solution temperature was monitored and recorded by an IR thermal camera (Ti125, Fluke, Everett, WA, USA). For the photothermal conversion efficiency test of as-prepared DG@TA-Fe^{III} NPs, 2 mL of DG@TA-Fe^{III} NPs were irradiated to reach the plateau of maximum temperature (58 °C), and finally the photothermal conversion efficiency was calculated to be around 36.1% according to the method reported elsewhere.

2.7. *In vitro biocompatibility evaluation of DG@TA-Fe^{III} NPs*

Human Umbilical Vein Endothelial Cells (HUVECs) were used here as a normal cell line to investigate the cytotoxicity of

DG@TA-Fe^{III} NPs by a standard MTT assay. For evaluating the hemocompatibility, gradient concentrations of DG@TA-Fe^{III} NPs were incubated with diluted healthy rabbit blood at 37 °C for 3 h. After centrifugation, the absorbance of supernatant at 450 nm was measured to calculate the relative percent hemolysis. The blood mixed with isosmotic normal saline and DI water was used as the negative and positive controls, respectively.

2.8. *Enhanced cellular uptake of DOX upon NIR laser irradiation*

Exponentially growing 4T1 cancer cells were seeded in 24-well culture plates with a density of 1×10^5 cells per well. After proliferation for 24 h, the culture medium was refreshed with 1 mL of RPMI 1640 containing DG@TA-Fe^{III} NPs (100 μg/mL) or free DOX with equivalent concentration of 1.1 μg/mL. The cells were then irradiated by an NIR laser (808 nm, 2 W/cm^2) immediately for 0, 3 and 5 min. Following a further incubation for 10 min, the cells were fixed with 4% of paraformaldehyde for 30 min and treated with 0.1% of Triton X-100/PBS (10 min) for enhanced permeabilization. After that, a standard nucleus staining assay was performed by incubating 4T1 cancer cells with 10 μg/mL of 4′,6-diamidino-2-phenylindole (DAPI). Finally, the intracellular uptake of DOX with various treatments after typical rinsing with PBS buffer was imaged by inverted fluorescence microscope.

2.9. *In vivo tumor inhibition study*

All animal experimental protocols were performed in accordance with the Guidelines for Care and Use of Laboratory Animals of Hefei University of Technology and approved by the Institutional Animal Care and Use Committee of Hefei University of Technology, Hefei, China.

Female BALB/c mice were subcutaneously injected with murine 4T1 cancer cells (1×10^6 cells per mouse, 100 μL) and randomly grouped when the tumor volume achieved to ~80 mm^3. The dosage of intravenously administered free DOX·HCl was 2 mg/kg. For DG@TA-Fe^{III} NPs-treated mice, the dosage of DG@TA-Fe^{III} NPs was 50 mg/kg with an equivalent DOX dosage of 0.5 mg/kg (10 mg/mL, 100 μL). Then, tumors were selectively illuminated with/without NIR laser (808 nm, 1 W/cm^2) for 10 min. After various treatments, the tumor volume and body weight of mice were recorded every other day as well as the characterizations of typical H&E histological and TUNEL immunofluorescent staining of tumor slices.

2.10. *Statistical analysis*

The data statistical analysis was carried out by using typical Student's *t*-test model. Data were expressed as mean ± SD, $n = 3$. Differences at $P < 0.01$ and $P < 0.001$ were considered statistically significant and highly significant, respectively.

3. Results and discussion

3.1. *Characterization of DG@TA-Fe^{III} NPs*

After mixing DOX and glutaraldehyde (GTA) molecules with various feeding ratio at room temperature for 2 h, the monodispersed gelatin NPs which developed from a well-reported two-step desolvation method were then quickly added into the aldehydated DOX solution[33,34]. Following 2-h intense agitation, the DG NPs could be collected by a typical centrifugation/rinsing process. As shown in Supporting Information Table S1 and Fig. S1, the content of covalently-linked DOX and diameter of obtained DG NPs were elevated as the feeding amount of GTA molecules increased, further confirmed by the gradually deepened pink solution color of DG NPs (inset of Fig. S1). Considering the delivery advantage of NPs with small size, optimized DG NPs with a feeding weight ratio of 1:50 of DOX *versus* GTA were thus chosen for further study.

Benefitting from the adhesive catechol chemistry[35,36], the polyphenol TA and Fe^{III} ions could be deposited successfully on the surface of DG NPs evidenced by the corresponding solution color change of obtained DG@TA and DG@TA-Fe^{III} NPs (Fig. 1A). In addition, the characteristic absorption peak at 276 nm of TA (assigned to the π-system of the benzene ring) was shifted and splited into two absorption peaks at 235 and 315 nm, further suggesting the formation of TA-Fe^{III} complex. As seen from Fig. 1B, the zeta potential of NPs was reversed from positive DG NPs (+15.9 mV) to negative DG@TA NPs (−13.7 mV) and DG@TA-Fe^{III} NPs (−24.8 mV), demonstrating the good packaging effect of TA-Fe^{III} shell with a slight increase in hydrodynamic diameter distribution (Fig. 1C). As seen from TEM and SEM images (Fig. 1D), the obtained DG@TA-Fe^{III} NPs exhibited monodispersed spherical morphologies with rough surfaces consisted of TA-Fe^{III} complex which were confirmed by the element mapping results (Fig. 1E).

Due to the protonated hydroxyl groups of TA molecules in acidic conditions, the TA and Fe^{III}-coordinated complex would dynamically transit from tris-, bis-to mono-analogues as evidenced by the stability constants of TA-Fe^{III} are 2.8×10^{17}, 3.4×10^9 and 1.5×10^5 at pH 8.0, 5.0 and 2.0, respectively[37]. This pH-dependent and dynamic binding performance urged us to investigate the storage stability of as-prepared DG@TA-Fe^{III} NPs. Due to the hydrophilic and negative charged surface, no significant change in hydrodynamic diameter and absorbance (808 nm) of DG@TA-Fe^{III} NPs could be observed in various mediums including DI water, PBS and RPMI-1640 cell culture medium with a pH value of 7.4 (Fig. 2A and B). In contrast, the absorbance of DG@TA-Fe^{III} NPs solution could be drastically decreased after incubating in acidic mediums (pH 5.0 and 6.0). The underlying mechanism was that the hydroxyl groups of TA molecules would be protonated at acidic conditions and partial of TA-Fe^{III} shells were then destabilized from the NPs' surface to not only expose the inner DG cores but also crosslink the neighboring NPs which consequently led to rapid aggregation of DG@TA-Fe^{III} NPs (Fig. 2C). Actually, although the increased diameter of DG@TA-Fe^{III} NPs may not be useful for promoting intracellular uptake by tumor cells, this acidic pH-induced unlock and aggregation are supposed to be beneficial for the long-retention and DOX release in mild acidic tumor microenvironment.

Next, the long-term storage stability of DG@TA-Fe^{III} NPs at pH 7.4 motivated us to test their cytotoxicity by standard methylthiazolyldiphenyl-tetrazolium bromide (MTT) and hemolytic procedures. Despite containing chemotherapeutic DOX molecules, the as-prepared DG@TA-Fe^{III} NPs still occupied good biocompatibility to HUVECs (used here as model normal cells) as the relative viability of HUVECs could reach 83.7 ± 3.1% after 24 h incubation with 600 μg/mL of DG@TA-Fe^{III} NPs, suggesting negligible DOX was released during the incubation (Supporting Information Fig. S2). In addition, after adding gradient

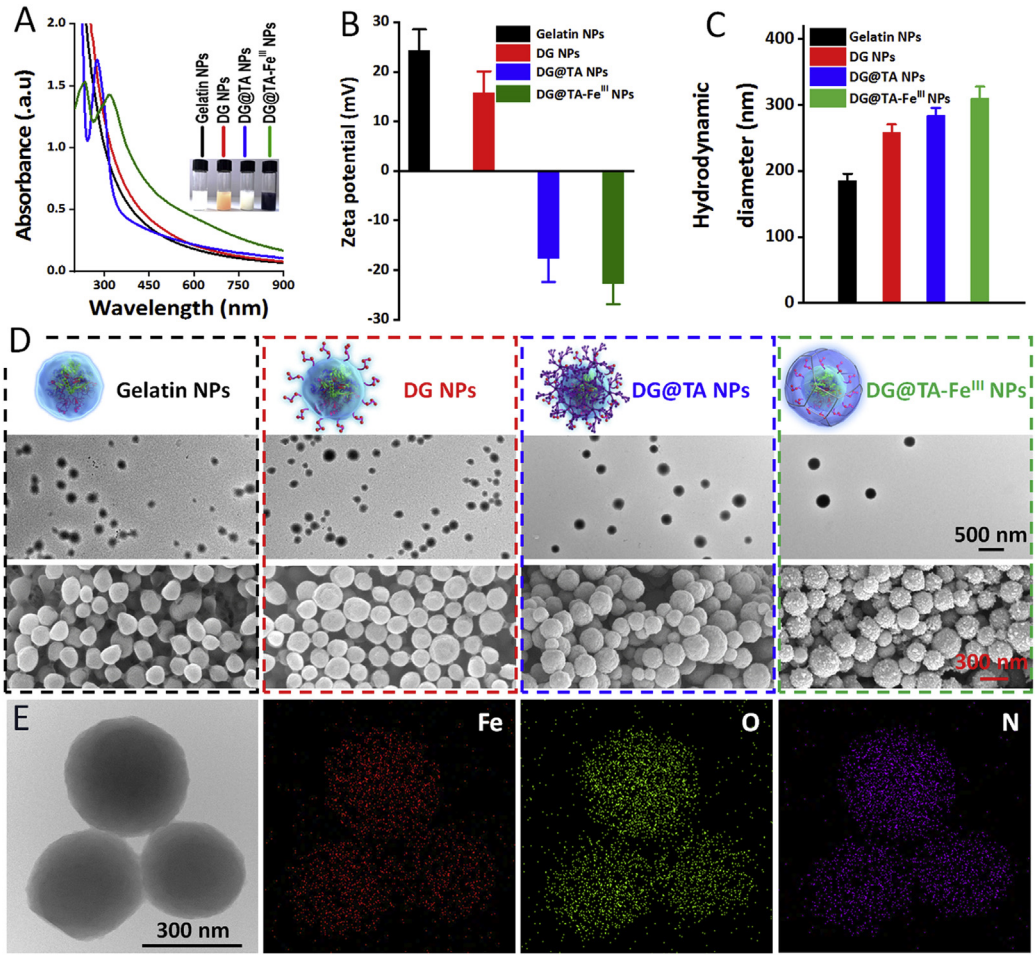

Figure 1 Characterization of as-prepared DG@TA-Fe^{III} NPs. (A) UV−Vis−NIR absorbance spectra (inset: photographs of corresponding NPs aqueous solution); (B) zeta potential and (C) average hydrodynamic diameter of freshly prepared NPs, data are expressed as mean ± SD (n = 3); (D) typical cartoon analogues, TEM and SEM images; (E) element mapping of DG@TA-Fe^{III} NPs.

concentrations of DG@TA-Fe^{III} NPs into freshly diluted rabbit blood for 3 h, all NPs incubated groups exhibited negligible percent hemolysis (less than 3%) which were comparable to negative control (isosmotic normal saline, Fig. 2D). Thus, all of the above data indicated the good biocompatibility of as-prepared DG@TA-Fe^{III} NPs which was essential for further biomedical application.

3.2. *"AND" logic gate-controlled DOX release*

According to our hypothesis, the cryptobiotic DG@TA-Fe^{III} NPs was expected to show negligible premature DOX leakage before arriving at tumor sites and "AND" logic gate-controlled DOX delivery by sequential disassembly of TA-Fe^{III} protective shell and enzymolysis of inner DG cores (Fig. 3A). To approve this "AND" logic gate performance, the pH and ATP-responsive disassembly behaviors of TA-Fe^{III} shell were firstly verified *in vitro*. By packaging DG@TA-Fe^{III} NPs which were dispersed in PBS with various pH or gradient concentrations of ATP in dialysis bags (MW = 14,000 Da), the concentrations of released iron were determined by a typical 1,10-phenanthroline chromogenic method[38]. As expected, as the stability constants of TA-Fe^{III} decreased when the solution became more acidic, nearly 47.8% and 84.3% of iron could be disassembled from protective TA-Fe^{III} shells for 12 h when DG@TA-Fe^{III} NPs were incubated in acidic PBS with a pH value of 6.0 and 5.0, respectively. In sharp contrast, only 9.8% of iron was released at pH 7.4 (Fig. 3B). Moreover, inspired by the upregulated level of ATP in cancerous tissues and stronger binding affinity of ATP-Fe^{III} than polyphenol-Fe^{III} coordination[39–41], the ATP-triggered disassembly of TA-Fe^{III} shell from DG@TA-Fe^{III} NPs was also investigated. As shown in Fig. 3C, the amount of iron released from DG@TA-Fe^{III} NPs was almost negligible in the absence of ATP, while it increased as not only the prolonged time but also elevated ATP dosage. Particularly, nearly 68.4% and 75.6% of iron could be destabilized from TA-Fe^{III} shells when mixing with 1.0 mg/mL of ATP for 4 and 12 h, respectively. Therefore, the specific and sensitive pH/ATP dependent TA-Fe^{III} shells disassembly was attractive for realizing minimized premature DOX leakage at circulated body fluids and potential burst DOX release at acidic and ATP-upregulated tumor microenvironment.

Motivated by the sensitive pH/ATP responsive disassembly of TA-Fe^{III} shells, DOX release profiles of totally naked DG NPs with or without gelatinase was evaluated subsequently *in vitro* (Fig. 3D). Upon addition of gelatinase (mimic MMP 2/9 in tumor region) for 12 h, around 82.1% of conjugated DOX could be quickly liberated from DG NPs which is over 6-fold increase *versus* the system without enzyme, suggesting the efficient enzymolysis of DG NPs

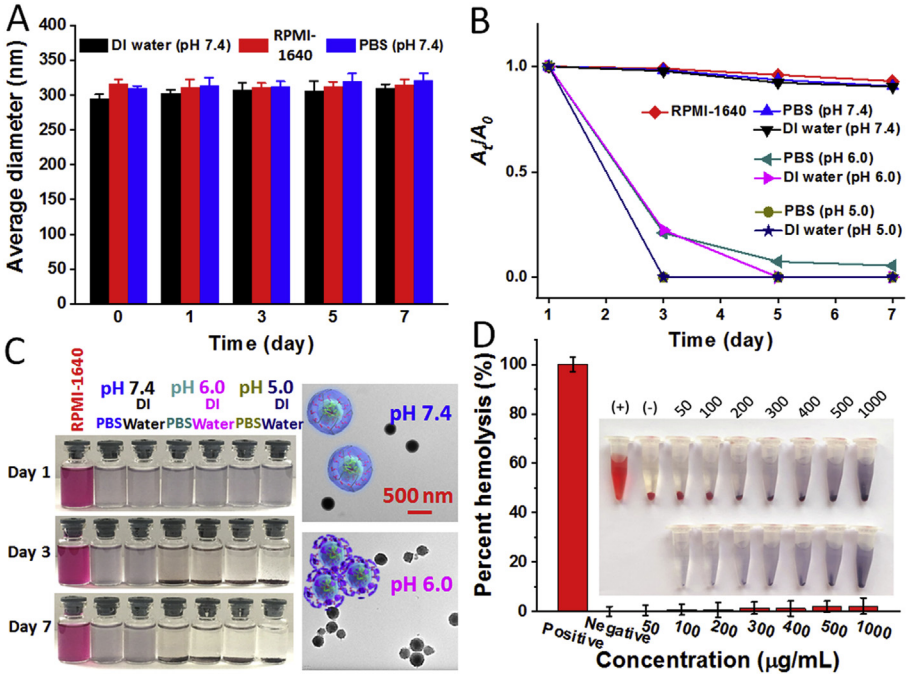

Figure 2 Stability and biocompatibility evaluation of DG@TA-Fe^{III} NPs. (A) Average hydrodynamic diameter and (B) relative absorbance at 808 nm of NPs in various medium for different days; (C) photographs and typical TEM images of aqueous NPs solutions with different pH; (D) hemolysis assay. Data are expressed as mean ± SD ($n = 3$).

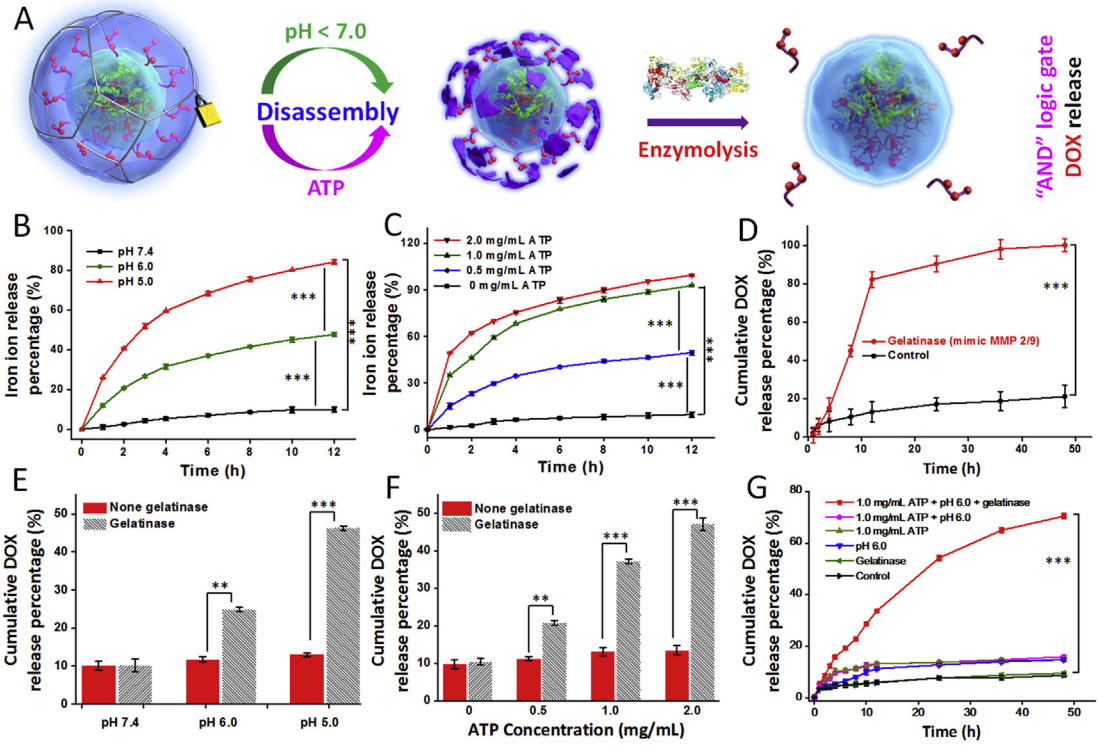

Figure 3 *In vitro* "AND" logic gate controlled DOX delivery performance. (A) Schematic illustration of sequential disassembly and enzymolysis process of DG@TA-Fe^{III} NPs; time-dependent release of Fe^{III} from DG@TA-Fe^{III} NPs at various (B) pH and (C) ATP concentration; (D) DOX release performance of DG NPs (3.0 mg/mL, 3.0 mL) with the enzymolysis of gelatinase; cumulative DOX release profiles from DG@TA-Fe^{III} NPs (1 mg/mL, 3.0 mL) under the assistance of various (E) pH and (F) ATP concentration; (G) cumulative DOX release profiles under various conditions. Data are expressed as mean ± SD ($n = 3$), $^{**}P < 0.01$, $^{***}P < 0.001$.

could be realized by gelatinase. Hence, the sequential "AND" logic gate-controlled DOX release from cryptobiotic DG@TA-Fe^{III} NPs was then further tested by synergistic TA-Fe^{III} shell disassembly (triggered by acidic pH or ATP) and DG core enzymolysis (sensitive to MMP 2/9). From Fig. 3E and F, although either acidic pH or ATP could unlock the TA-Fe^{III} shells, nearly no conjugated DOX molecules would be released without the assistance of gelatinase. Equally, it seems also impossible for gelatinase to directly cut off DOX molecules from DG@TA-Fe^{III} NPs due to the hinder effect of intact TA-Fe^{III} shells, indicating a significant sequential "AND" logic gate-based drug release profile. Moreover, to mimic the coexistence of acidic pH and upregulated ATP level, the simultaneous disassembly of TA-Fe^{III} shells by ATP and acidic pH would provide more chances for gelatinase to hydrolyze inner DG cores (Fig. 3G), consequently resulting in facilitated cytotoxic DOX release which is beneficial for tumor-targeted drug delivery with minimized adverse effects.

3.3. *Enhanced cellular uptake of DOX under NIR light irradiation*

In light of the well-reported phenomenon that hyperthermia would promote cellular uptake of chemotherapeutic drug by accelerated cell metabolism and membrane fluidity[42], the concentration-dependent broad UV−Vis−NIR absorption spectra of DG@TA-Fe^{III} NPs solution which dispersed either in DI water or RPMI-1640 cell culture medium not only suggested its good dispersity but also encouraged us to evaluate the photothermal conversion efficiency (Fig. 4A and Supporting Information S3). As expected, DG@TA-Fe^{III} NPs possessed good photothermal conversion capacity derived from their photosensitive TA-Fe^{III} shells with both NPs' dosage and power density of incident NIR light dependent manners (Fig. 4B and C). For instance, exposing DG@TA-Fe^{III} NPs solution (200 μL) with gradient concentrations of 50, 100, 150, 200, 300 and 400 μg/mL to NIR light (808 nm, 2.0 W/cm^2)

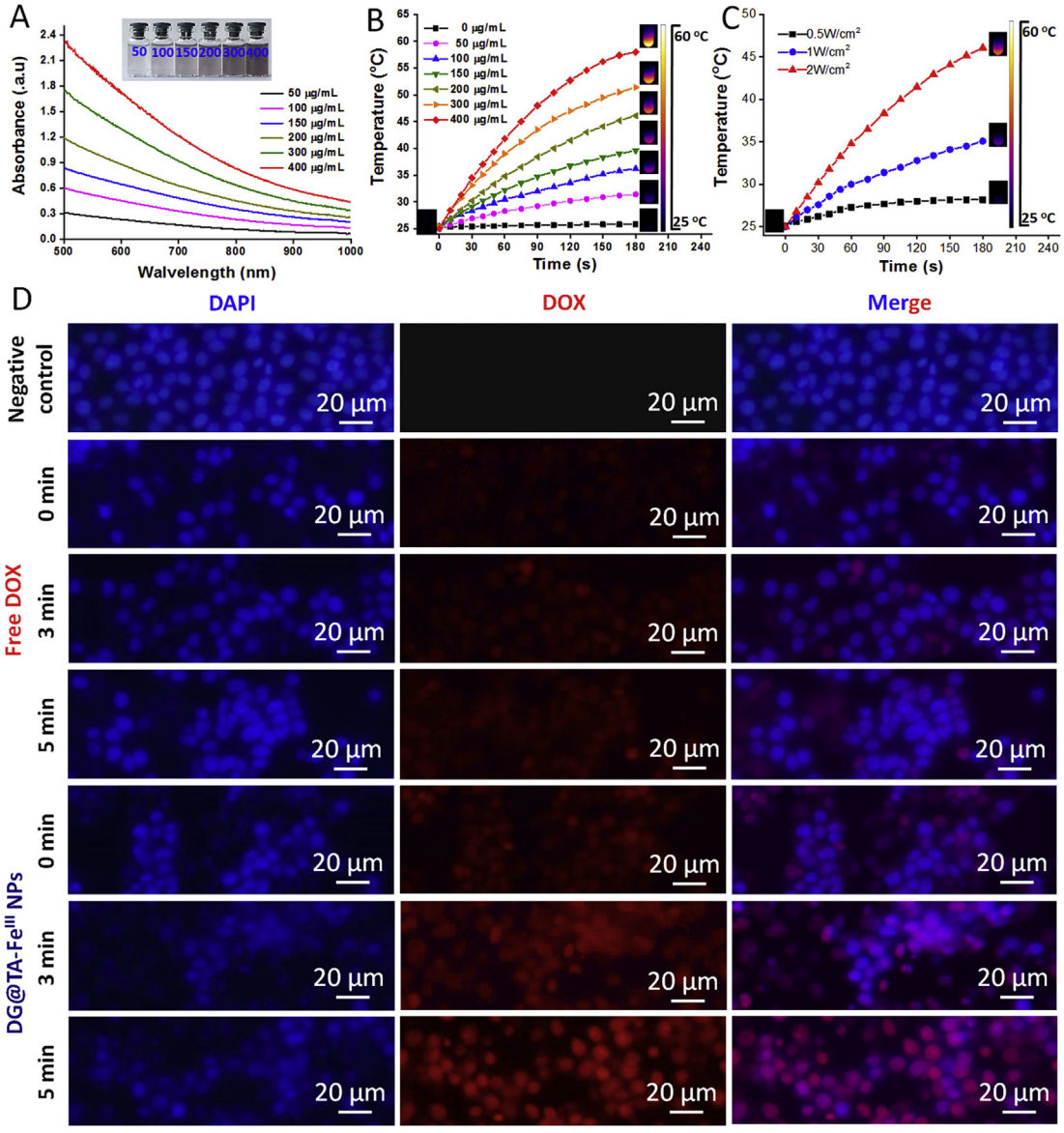

Figure 4 (A) UV−Vis−NIR absorption spectra and photograph (inset) of gradient concentrations of DG@TA-Fe^{III} NPs aqueous solution; photothermal conversion effect which depended on (B) NPs dosage and (C) power density of incident NIR light; (D) fluorescent images of 4T1 cancer cells with various treatments.

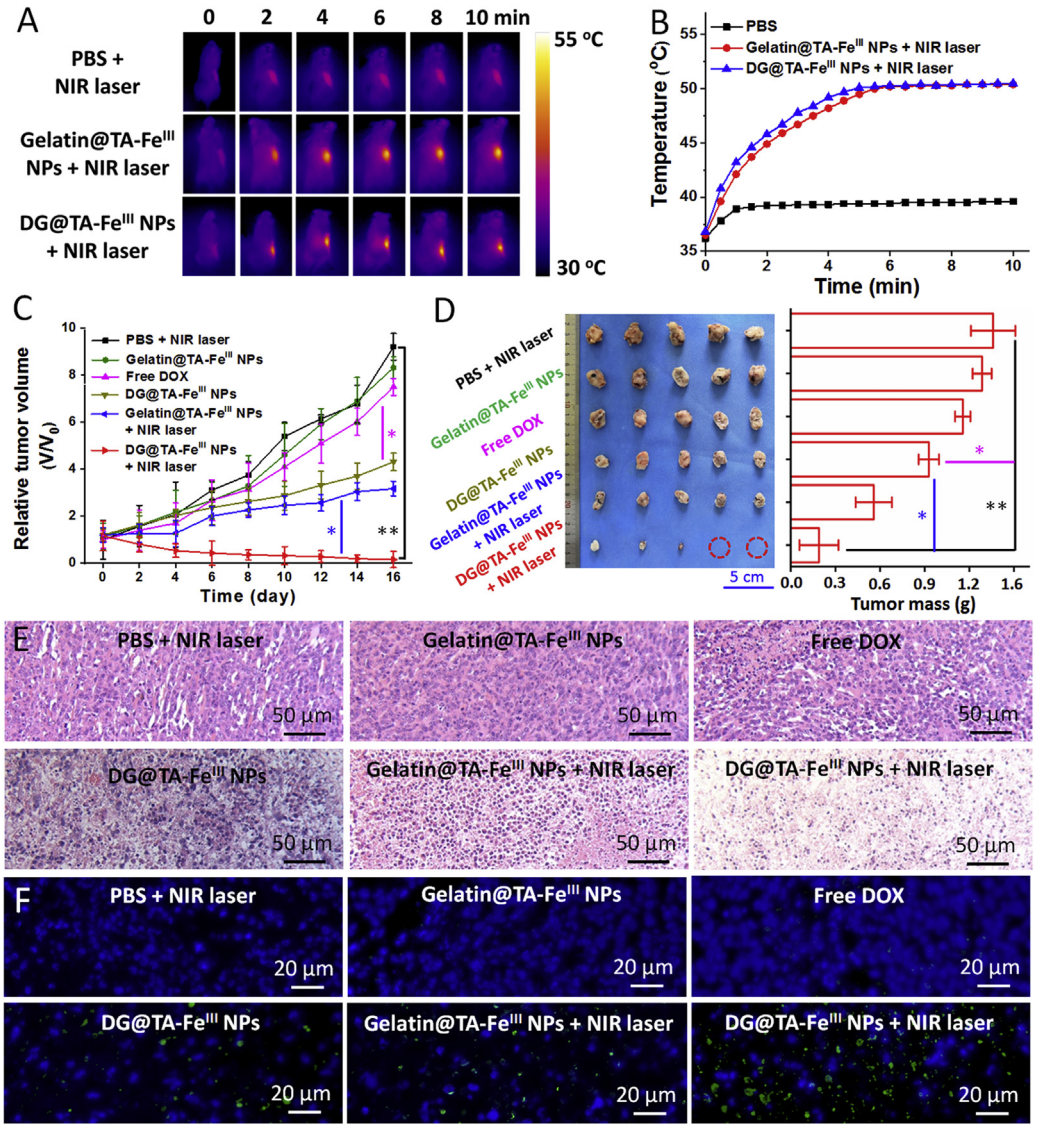

Figure 5 Characterization of synergistic tumor inhibition *in vivo* from DG@TA-Fe^{III} NPs under the assistance of NIR laser irradiation. (A) IR thermal images and (B) quantized tumor temperature changes; (C) relative tumor volume and (D) photograph of dissected tumor samples as well as tumor weight at 16th day after various treatments as indicated, data are expressed as mean ± SD ($n = 5$); (E) H&E histological analysis and (F) TUNEL immunofluorescence characterizations of dissected tumor samples with various treatments; $^{*}P < 0.05$, $^{**}P < 0.01$.

for 3 min would elevated the solution temperature from 25 to 31.4, 36.2, 39.6, 46.1, 51.4 and 58 °C, respectively, while only 0.8 °C temperature rise was observed for DI water. In addition, the considerable photothermal stability and conversion efficiency (around 36.1%) suggested that DG@TA-Fe^{III} NPs could act as an efficient photothermal agent (Supporting Information Fig. S4).

Chemocytotoxic DOX molecules were covalently conjugated to the gelatin NPs through typical aldimine condensation without forming any thermo-sensitive bonds which led to the non-thermo responsive DOX release performance from DG NPs (Supporting Information Fig. S5). Nevertheless, the well-known heat-promoted cellular uptake of drug inspired us to investigate the possibility of accelerated DOX internalization induced by DG@TA-Fe^{III} NPs under NIR laser illumination. As shown in Fig. 4D and Supporting Information Fig. S6, no significant difference on cellular uptake of free DOX (1.1 μg/mL) could be observed with NIR laser irradiation (808 nm, 2.0 W/cm^2) for 0, 3 and 5 min. In contrast, a steady increase of DOX fluorescence was found in 4T1 cells treated with 100 μg/mL of DG@TA-Fe^{III} NPs and NIR light illumination. Thus, benefiting from the controlled tumor-targeted NIR laser irradiation, DG@TA-Fe^{III} NPs would be anticipated to exhibit a noteworthy synergistic cancer cell killing effect.

3.4. *In vivo synergistic tumor inhibition*

After evaluating the localized photothermal ablative capacity of DG@TA-Fe^{III} NPs by a well-reported Live/Dead cell staining assay (Supporting Information Fig. S7), the synergistic PTT-chemo cancer cell killing efficiency resulted from DG@TA-Fe^{III} NPs plus NIR light illumination was further evaluated *in vivo* by using 4T1 tumor xenograft in BALB/c female mice. Randomly grouped mice ($n = 8$) with average tumor volume of ~80 mm^3 were treated with PBS + NIR laser, Gelatin@TA-Fe^{III} NPs, free

DOX, DG@TA-Fe^{III} NPs, Gelatin@TA-Fe^{III} NPs + NIR laser and DG@TA-Fe^{III} NPs + NIR laser, respectively. Upon 10 min of tumor-targeted NIR laser irradiation (808 nm, 1.0 W/cm^2), the localized tumor temperature of PBS treated group was only slightly increased to 38.9 °C, demonstrating the safety of incident light. In contrast, owing to the good photothermal conversion ability of TA-Fe^{III} shells, the temperature of tumor treated with Gelatin@TA-Fe^{III} NPs and DG@TA-Fe^{III} NPs could locally achieved to around 50.2 and 50.4 °C, respectively (Fig. 5A and B).

The tumor volume of mice was monitored every other day to evaluate the therapeutic efficiency. As shown in Fig. 5C, the tumors treated with PBS + NIR laser and Gelatin@TA-Fe^{III} NPs showed fast proliferating behaviors within 16 days, while quadruple free DOX (2.0 mg/kg) was also shown slight tumor inhibition effect due to poor tumor accumulation and the low dosage used here. For the mice treated with Gelatin@TA-Fe^{III} NPs + NIR laser and DG@TA-Fe^{III} NPs, notable tumor inhibition but subsequent recurrence occurred due to insufficient generated heat and dosage of released DOX in this study. Satisfactorily, nearly completely tumor inhibition and no recurrence occurred in the following 16 days were achieved in DG@TA-Fe^{III} NPs + NIR laser group, indicating a synergistic cancer cell killing effect by combined photothermal–chemo therapy (Fig. 5D and Supporting Information Fig. S8).

Typical H&E histological (Fig. 5E) and TUNEL immunofluorescent staining (Fig. 5F) of tumor slices in various treated groups were further carried out. No significant morphological changes and TUNEL signals (green fluorescence) were observed in PBS + NIR laser and Gelatin@TA-Fe^{III} NPs groups. In comparison to free DOX-treated tumors, more cytoplasm shrinking and TUNEL signals could be found in DG@TA-Fe^{III} NPs group due to the tumor targeted burst release of cytotoxic DOX molecules. As expected, DG@TA-Fe^{III} NPs + NIR laser group present the most serious cell destruction and TUNEL signals in tumor cells owing to the synergistic photothermal–chemo effect. Moreover, the characterizations of body weight (Supporting Information Fig. S9) and major organ histological analysis (Supporting Information Fig. S10) suggested that no significant side effects would be induced by DG@TA-Fe^{III} NPs as well as NIR laser illumination. Therefore, cryptobiotic DG@TA-Fe^{III} NPs would occupy promising tumor-preferred cytotoxicity due to “AND” logic gate-controlled DOX delivery as well as synergistic photothermal–chemo effect with the assistance of NIR laser irradiation.

4. Conclusions

Inspired by the natural cryptobiosis with environment sensitive shells and polyphenol–metal coordination chemistry, DG@TA-Fe^{III} NPs were successfully developed here as a “AND” logic gate nanoplatform for controlled DOX delivery. Benefiting from the altered tumor microenvironment, DG@TA-Fe^{III} NPs would go through a TA-Fe^{III} shells disassembly by acidic pH/ATP and subsequent enzymolysis of inner DOX-conjugated DG cores to realize tumor-specific DOX release with minimized premature drug leakage in surrounding healthy tissues. Moreover, the photothermal conversion ability of TA-Fe^{III} complex also endowed DG@TA-Fe^{III} NPs good potential for synergistic photothermal–chemo tumor inhibition. Therefore, our study presented a simple strategy for developing crytobiotic “AND” logic gate nanoplatform with tumor-specific drug delivery by forming polyphenol–metal complexes on enzyme degradable drug conjugates.

Acknowledgments

This work was financially supported by the Shenzhen Science and Technology Programs (No. JYCJ20170413165233512, China), University Synergy Innovation Program of Anhui Province (No. GXXT-2019-045, China) and the Fundamental Research Funds for the Central Universities (No. JZ2018HGPA0273, China).

Author contributions

Ping Jin and Zhengbao Zha designed the research. Hu Zhou and Gang He carried out the experiments and performed data analysis. Yanbin Sun, Jingguo Wang and Haitao Wu participated part of the experiments. Zhengbao Zha wrote the manuscript. Ping Jin revised the manuscript. All of the authors have read and approved the final manuscript.

Conflicts of interest

The authors have no conflicts of interest to declare.

Appendix A. Supporting information

Supporting data to this article can be found online at https://doi.org/10.1016/j.apsb.2020.08.007.

References

1. Badeau BA, Comerford MP, Arakawa CK, Shadish JA, DeForest CA. Engineered modular biomaterial logic gates for environmentally triggered therapeutic delivery. *Nat Chem* 2018;**10**:251−8.
2. Mura S, Nicolas J, Couvreur P. Stimuli-responsive nanocarriers for drug delivery. *Nat Mater* 2013;**12**:991−1003.
3. Hoffman AS. Stimuli-responsive polymers: biomedical applications and challenges for clinical translation. *Adv Drug Deliv Rev* 2013;**65**:10−6.
4. Min Y, Caster JM, Eblan MJ, Wang AZ. Clinical translation of nanomedicine. *Chem Rev* 2015;**115**:11147−90.
5. Li C, Wang JC, Wang YG, Gao HL, Wei G, Huang YZ, et al. Recent progress in drug delivery. *Acta Pharm Sin B* 2019;**9**:1145−62.
6. He G, Chen S, Xu YJ, Miao ZH, Ma Y, Qian HS, et al. Charge reversal induced colloidal hydrogel acts as a multi-stimuli responsive drug delivery platform for synergistic cancer therapy. *Mater Horiz* 2019;**6**:711−6.
7. Sawaya RE, Yamamoto M, Gokaslan ZL, Wang SW, Mohanam S, Fuller GN, et al. Expression and localization of 72 kDa type IV collagenase (MMP-2) in human malignant gliomas *in vivo*. *Clin Exp Metastasis* 1996;**14**:35−42.
8. Radhakrishnan K, Tripathy J, Raichur AM. Dual enzyme responsive microcapsules simulating an “OR” logic gate for biologically triggered drug delivery applications. *Chem Commun* 2013;**49**:5390−2.
9. Zha Z, Zhang S, Deng Z, Li Y, Li C, Dai Z. Enzyme-responsive copper sulphide nanoparticles for combined photoacoustic imaging, tumor-selective chemotherapy and photothermal therapy. *Chem Commun* 2013;**49**:3455−7.
10. Cheng R, Meng FH, Deng C, Klok HA, Zhong ZY. Dual and multi-stimuli responsive polymeric nanoparticles for programmed site-specific drug delivery. *Biomaterials* 2013;**34**:3647−57.
11. Qu Y, Chu B, Wei X, Lei M, Hu D, Zha R, et al. Redox/pH dual-stimuli responsive camptothecin prodrug nanogels for "on-demand" drug delivery. *J Control Release* 2019;**296**:93−106.
12. Li Y, Li Y, Zhang X, Xu X, Zhang Z, Hu C, et al. Supramolecular PEGylated dendritic systems as pH/redox dual-responsive theranostic

nanoplatforms for platinum drug delivery and NIR imaging. *Theranostics* 2016;**6**:1293−305.
13. Ang CY, Tan SY, Teh C, Lee JM, Wong MF, Qu Q, et al. Redox and pH dual responsive polymer based nanoparticles for *in vivo* drug delivery. *Small* 2017;**13**. 1602379.
14. Ding J, Xiao C, Yan L, Tang Z, Zhuang X, Chen X, et al. pH and dual redox responsive nanogel based on poly(L-glutamic acid) as potential intracellular drug carrier. *J Control Release* 2011;**152**:e11−3.
15. Karimi M, Ghasemi A, Zangabad PS, Rahighi R, Basri SMM, Mirshekari H, et al. Smart micro/nanoparticles in stimulus-responsive drug/gene delivery systems. *Chem Soc Rev* 2016;**45**:1457−501.
16. Amir RJ, Popkov M, Lerner RA, Barbas III CF, Shabat D. Prodrug activation gated by a molecular "OR" logic trigger. *Angew Chem Int Ed* 2005;**44**:4378−81.
17. Bai L, Wang XH, Song F, Wang XL, Wang YZ. "AND" logic gate regulated pH and reduction dual-responsive prodrug nanoparticles for efficient intracellular anticancer drug delivery. *Chem Commun* 2015;**51**:93−6.
18. Yang B, Zhang XB, Kang LP, Huang ZM, Shen GL, Yu RQ, et al. Intelligent layered nanoflare: "lab-on-a-nanoparticle" for multiple DNA logic gate operations and efficient intracellular delivery. *Nanoscale* 2014;**6**:8990−6.
19. Wen Y, Xu L, Li C, Du H, Chen L, Su B, et al. DNA-based intelligent logic controlled release systems. *Chem Commun* 2012;**48**:8410−2.
20. Chao J, Liu H, Su S, Wang L, Huang W, Fan C. Structural DNA nanotechnology for intelligent drug delivery. *Small* 2014;**10**:4626−35.
21. Wei C, Guo J, Wang C. Dual stimuli-responsive polymeric micelles exhibiting "AND" logic gate for controlled release of adriamycin. *Macromol Rapid Commun* 2011;**32**:451−5.
22. Yan CX, Guo ZQ, Liu YJ, Shi P, Tian H, Zhu WH. A sequence-activated AND logic dual-channel fluorescent probe for tracking programmable drug release. *Chem Sci* 2018;**9**:6176−82.
23. Park JH, Hong D, Lee J, Choi IS. Cell-in-shell hybrids: chemical nanoencapsulation of individual cells. *Accounts Chem Res* 2016;**49**:792−800.
24. Clegg JS. Cryptobiosis—a peculiar state of biological organization. *Comp Biochem Physiol B* 2001;**128**:613−24.
25. Soemme L. Anhydrobiosis and cold tolerance in tardigrades. *Eur J Entomol* 1996;**93**:349−58.
26. McKenney PT, Driks A, Eichenberger P. The *Bacillus subtilis* endospore: assembly and functions of the multilayered coat. *Nat Rev Microbiol* 2013;**11**:33−44.
27. Foissner W. The stunning, glass-covered resting cyst of maryna umbrellata (Ciliophora, Colpodea). *Acta Protozool* 2009;**48**:223−43.
28. Yang SH, Hong D, Lee J, Ko EH, Choi IS. Artificial spores: cytocompatible encapsulation of individual living cells within thin, tough artificial shells. *Small* 2013;**9**:178−86.
29. Hong D, Park M, Yang SH, Lee J, Kim YG, Choi IS. Artificial spores: cytoprotective nanoencapsulation of living cells. *Trends Biotechnol* 2013;**31**:442−7.
30. Lee J, Choi J, Park JH, Kim MH, Hong D, Cho H, et al. Cytoprotective silica coating of individual mammalian cells through bioinspired silicification. *Angew Chem Int Ed* 2014;**53**:8056−9.
31. Lee J, Cho H, Choi J, Kim D, Hong D, Park JH, et al. Chemical sporulation and germination: cytoprotective nanocoating of individual mammalian cells with a degradable tannic acid−Fe^{III} complex. *Nanoscale* 2015;**7**:18918−22.
32. Park JH, Kim K, Lee J, Choi JY, Hong D, Yang SH, et al. A cytoprotective and degradable metal-polyphenol nanoshell for single-cell encapsulation. *Angew Chem Int Ed* 2014;**53**:12420−5.
33. Wong C, Stylianopoulos T, Cui J, Martin J, Chauhan VP, Jiang W, et al. Multistage nanoparticle delivery system for deep penetration into tumor tissue. *Proc Natl Acad Sci U S A* 2011;**108**:2426−31.
34. Diba M, Wang H, Kodger TE, Parsa S, Leeuwenburgh SCG. Highly elastic and self-healing composite colloidal gels. *Adv Mater* 2017;**29**. 1604672.
35. Ejima H, Richardson JJ, Liang K, Best JP, van Koeverden MP, Such GK, et al. One-step assembly of coordination complexes for versatile film and particle engineering. *Science* 2013;**341**:154−7.
36. He G, Yan X, Miao ZH, Qian HS, Ma Y, Xu Y, et al. Anti-inflammatory catecholic chitosan hydrogel for rapid surgical trauma healing and subsequent prevention of tumor recurrence. *Chin Chem Lett* 2020;**31**:1807−11.
37. Sungur Ş, Uzar A. Investigation of complexes tannic acid and myricetin with Fe (III). *Spectrochim Acta* 2008;**69**:225−9.
38. Zhang L, Wan SS, Li CX, Xu L, Cheng H, Zhang XZ. An adenosine triphosphate-responsive autocatalytic Fenton nanoparticle for tumor ablation with self-supplied H_2O_2 and acceleration of Fe (III)/Fe (II) conversion. *Nano Lett* 2018;**18**:7609−18.
39. Zhou Y, Tozzi F, Chen J, Fan F, Xia L, Wang J, et al. Intracellular ATP levels are a pivotal determinant of chemoresistance in colon cancer cells. *Canc Res* 2012;**72**:304−14.
40. Chung JE, Tan S, Gao SJ, Yongvongsoontorn N, Kim SH, Lee JH, et al. Self-assembled micellar nanocomplexes comprising green tea catechin derivatives and protein drugs for cancer therapy. *Nat Nanotechnol* 2014;**9**:907−12.
41. Song XR, Li SH, Dai J, Song L, Huang G, Lin R, et al. Polyphenol-inspired facile construction of smart assemblies for ATP- and pH-responsive tumor MR/optical imaging and photothermal therapy. *Small* 2017;**13**. 1603997.
42. Chen HJ, Ma Y, Wang XW, Zha ZB. Multifunctional phase-change hollow mesoporous Prussian blue nanoparticles as a NIR light responsive drug co-delivery system to overcome cancer therapeutic resistance. *J Mater Chem B* 2017;**5**:7051−8.